AUXILIARY MATERIAL
Effects of Planet Curvature and Crust on the Shock Pressure Field around Impact Basins

Karin L. Louzada, Sarah T. Stewart

Department of Earth and Planetary Sciences, Harvard University, Cambridge, MA, USA.

The auxiliary material for this article contains:

1. Figure S1: Calculations of ray path lengths for direct and reflected waves in a flat and spherical geometry.
2. Figure S2: The internal structure models for Mars.
3. Figure S3: Timestep, angle spacing and grid size sensisivity tests for the ray path model (including Table S1).
4. Description of the CTH calculations (including Table S2).
5. Table S3: Input variables for Figure 3 in the main text.
6. Figure S4: Crust-mantle boundary effects.
7. Figure S5: Evolution of the burial depth in CTH simulations.
8. Table S4: Average shock pressures in the magnetic crust of Mars for a Hellas-type event.

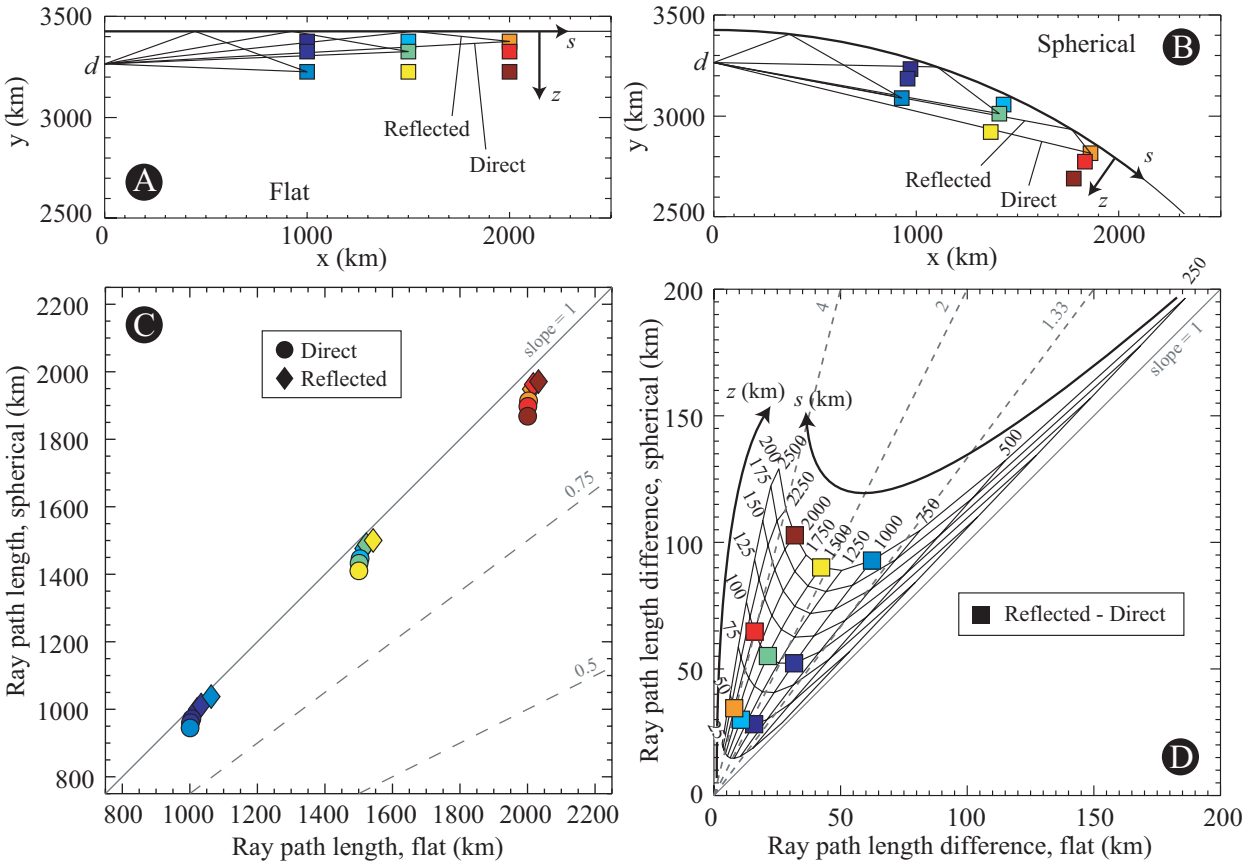

Figure S1. Direct and reflected ray paths to selected locations in at distances along the surface, *s*, (1000, 1500, and 2500 km) and depths, *z*, (50, 100, 200 km) in a (A) flat and (B) spherical homogeneous (case I) Mars . The radius of Mars is 3426 km and the burial depth is 0.7·230 km. Three example direct and reflected ray paths are drawn in both panels to show the difference in the shape of the ray paths. (C) The calculated lengths of the direct (circles) and reflected (diamonds) ray paths in the flat versus the spherical case for each are shown. As expected, the direct and reflected ray paths are shorter in the spherical planet case. (D) The difference between the reflected and direct ray path lengths for flat versus spherical planet geometries. The ray path length difference is proportional to the arrival time difference of the waves. Ray path length differences are shorter in the flat planet case, increasing with distance *s* along the surface and decreasing with depth *z*. At 1000 km from the impact, at 50 km depth (the lower limit of the crustal thickness) the ray path length difference (and the arrival time difference) is 2 times greater in the spherical planet case than it is in the flat planet case (darkest blue square).

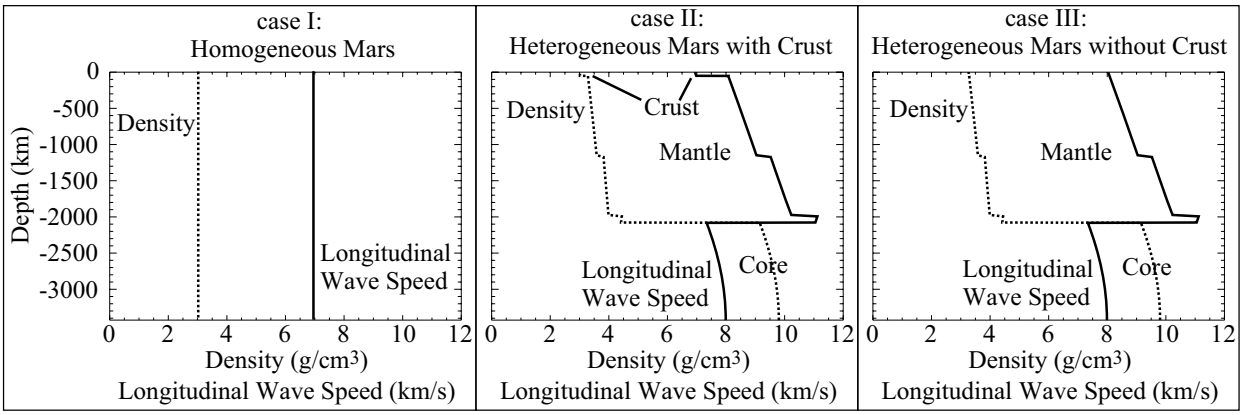

Figure S2. Internal structure models for Mars used in the ray-path and CTH calculations showing the change in density (dashed, courtesy of D. Valencia using the techniques described in [*Valencia, et al.*, 2006]) and longitudinal wave speed (black, scaled to the Preliminary Reference Earth Model, [*Dziewonski and Anderson*, 1981]). Three possible internal structures were considered: (I) homogeneous planet with a constant crustal density and sound speed. (II) a full heterogeneous Mars with a 50-km thick crust (3 g/cm^3) overlying a 2000-km thick mantle and core of 1376-km radius [*Zuber*, 2001], and (III), similar to (II) but without a crust. Phase transitions in the heterogeneous Mars occur at 1173 and 2126 km depth where olivine transforms to wadsleyite and ringwoodite transforms to perovskite and magnesiowüstite, respectively. The presence of the second transition is sensitive to the mass of the core (15% of the planet in this case). The radius of Mars is 3426 km.

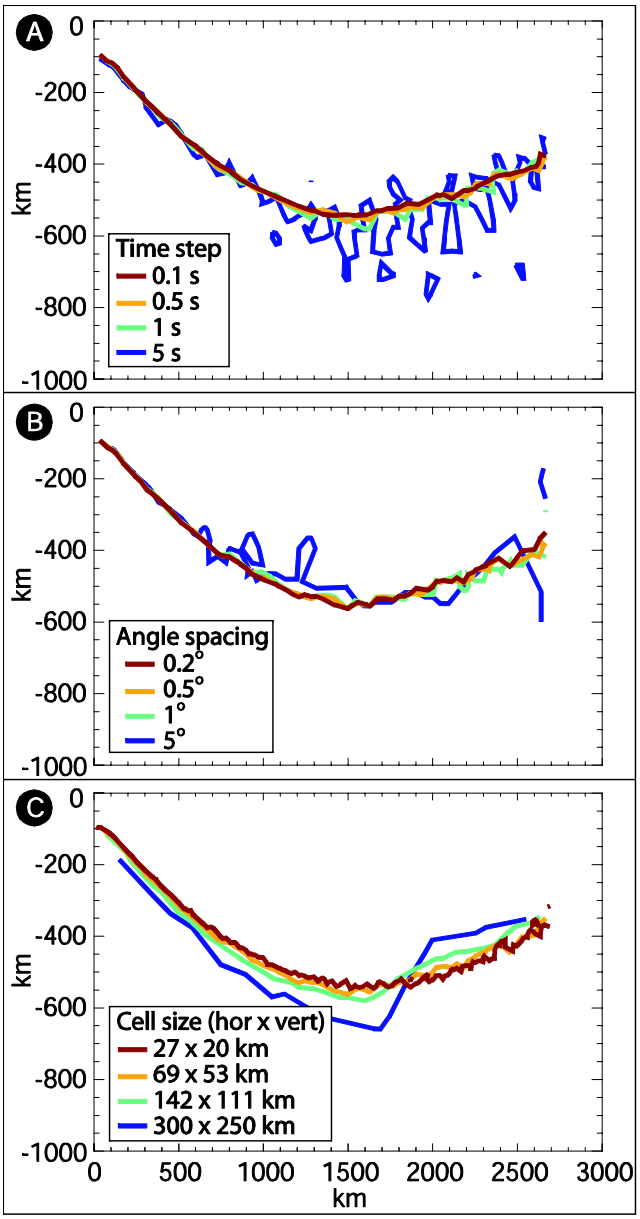

Figure S3. Tests evaluating the effects of (**A**) timestep, (**B**) angle spacing of rays emitted from the equivalent burial depth (the number of rays is indicated in Table S1), and (**C**) cell size in which the first arrivals of compressive and tensile waves are collected, on the location of the interference zone boundary. In each calculation the projectile radius is 230 km, the impact velocity is 9 km/s (vertical) and the planet geometery is spherical, using the Mars interior structure from Figure 2S. The remaining variables are indicated in Table S1. Vertical exaggeration = 2x.

Table S1. Variable input into the ray-path calculations in Figure S3, projectile radius is 230 km, the impact velocity is 9 km/s (vertical) and the planet geometery is spherical.

Panel –Color	*Timestep, seconds*	*Angle Spacing, degrees (number of rays)*	*Cell Size,km x km (hor x vert)*
A – Red	0.1	0.5 (360)	69 x 53
A – Orange	0.5	0.5 (360)	69 x 53
A – Green	1	0.5 (360)	69 x 53
A – Blue	5	0.5 (360)	69 x 53
B – Red	0.5	0.2 (900)	69 x 53
B – Orange	0.5	0.5 (360)	69 x 53
B – Green	0.5	1 (180)	69 x 53
B – Blue	0.5	5 (36)	69 x 53
C – Red	0.5	0.2 (900)	27 x 20
C – Orange	0.5	0.2 (900)	69 x 53
C – Green	0.5	0.2 (900)	142 x 111
C – Blue	0.5	0.2 (900)	300 x 250

Description of CTH calculations

CTH is an Eulerian shock physics code with multiple materials, adaptive mesh refinement, and Lagrangian tracer particles [*McGlaun, et al.*, 1990] that has been widely used in impact cratering studies. CTH version 8 has the option to include self-gravitational forces, using the parallel tree method of Barnes and Hut [1986]. We utilized tabulated equations of state [Sesame tables, see *Holian*, 1984]: projectile and crust – SiO_2 ANEOS [*Melosh*, 2007]; mantle –dunite ANEOS [*Benz, et al.*, 1989]; core – iron multiphase model [*Kerley*, 1993]. Mars was initialized with a geothermal profile (corresponding to the internal structure model in Figure S2) and three layers in gravitational equilbrium with radii of 1345, 3372, 3426 km for the core, mantle and crust, respectively. In some cases, the crust was omitted. All materials were hydrodynamic for a straightforward comparison to the wave propagation model; hence the final basin diameters were not calculated

The projectile was initialized in self-gravitational equilibrium for 3D runs and at zero pressure for 2D runs at a constant temperature of 200 K. Impacts were normal to the surface at 9 km/s. Lagrangian tracer particles were placed in the impact plane (2D tracer distribution in all cases) with greater spatial resolution near the impact point and in the crust (an example tracer distribution is shown in Figure 2).

The spatial resolution of the Eulerian grid was highest near the impact point and in the impact plane, and decreases with distance. Note that the adaptive mesh refinement scheme in CTH keeps materials adjacent to highly resolved regions at the same resolution or decreased by a factor of 2 [*Crawford*, 1999].

Table S2. Overview of CTH calculations.

Simulation Geometry	*Projectile Radius* (km)	*Mars Layers*	*Projectile Resolution* (km)	*Crust Resolution* (km)	*Mantle Resolution* (km)	*Figures*
2D	230	Mantle, core	5	----	1.25	S4C, S5B
2D	230	Crust, mantle, core	2.5	1.25	2.5	2, 4A, S4C, S5B
3D*	230	Crust, mantle, core	7.3	3.6	14.6	2, 4B, 4C, S4A, S5B
2D	125	Crust, mantle, core	2.5	1.25	2.5	
3D	125	Crust, mantle, core	3.6	3.6	14.6	4C
2D	50	Crust, mantle, core	1.3	0.63	1.25	S5B

*A 230-km radius projectile 3D case at about two times lower resolution in the projectile and crust yielded nearly identical results.

Table S3. Variables input into the ray-path calculations in Figure 3 (main text).

Projectile Radius, km	*Projectile/Mars Radius*	*Time Step, seconds*	*Angle Spacing, degrees (number of rays)*	*Cell Size, km x km (hor x vert)*
Heterogeneous Mars with Crust (red/pink)				
230	0.067	0.5	0.5 (360)	51.20 x 46.93
175	0.051	0.5	0.5 (360)	37.75 x 36.73
100	0.029	0.5	0.5 (360)	24.48 x 24.48
25	0.0072	0.1	0.1 (1800)	6.12 x 4.08
10	0.0029	0.1	0.1 (1800)	2.44 x 2.44
5	0.0014	0.1	0.1 (1800)	1.22 x 1.22
Homogeneous Mars (blue/light-blue)				
230	0.067	1	1 (180)	25.25 x 20.40
175	0.051	0.5	1 (180)	20.20 x 20.40
100	0.029	0.5	0.5 (360)	21.18 x 15.30
50	0.014	0.5	0.5 (360)	10.2 x 10.2
25	0.0072	0.1	0.5 (360)	6.12 x 6.12
10	0.0029	0.05	0.1 (1800)	2.04 x 2.04
5	0.0014	0.05	0.5 (360)	1.53 x 1.53

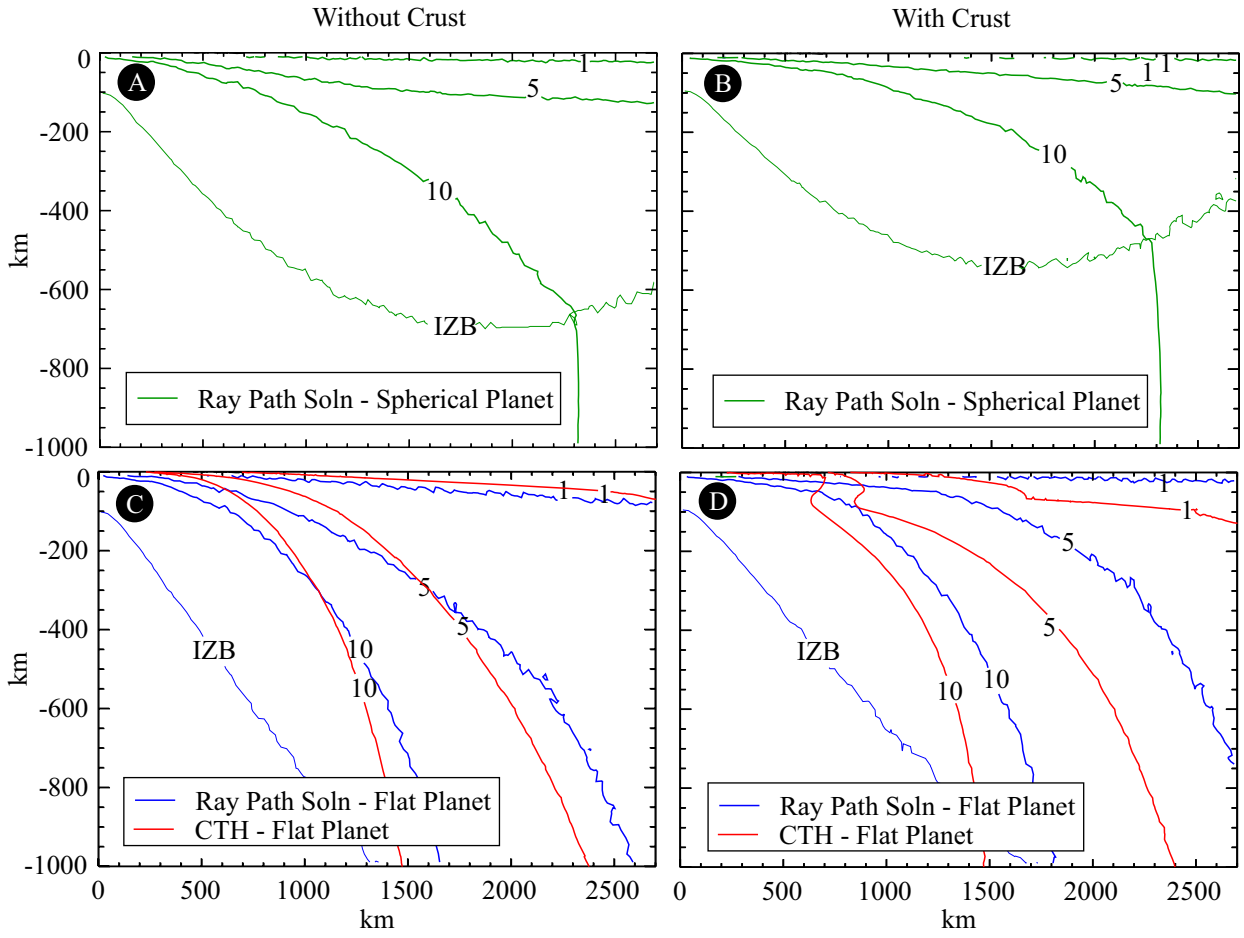

Figure S4. Tests showing the effect of including a crust in the internal structure of the planet on the peak shock pressure contours (1, 5 and 10 GPa) in (A, B) a spherical planet using the ray path solution and in (C, D) a flat planet using the ray path solution and CTH. The input variables are: projectile radius = 230 km, impact velocity = 9 km/s (vertical), time step = 0.5 s, ray spacing = 0.2 degrees, grid size = 27 x 20 km. The addition of a crust leads to shallowing of peak pressure contours near the surface in both the flat and spherical ray path calculations. The pressure contours in the ray path model for a planet without crust (B, solid) are similar to the pressure contours in the CTH calculation without crust (C, solid). The inclusion of a crust in the CTH simulation results in more complicated pressure contours (C, dashed). We infer that the ray path model does not accurately capture the effcets of the crust-mantle boundary. Vertical exaggeration = 1.7x.

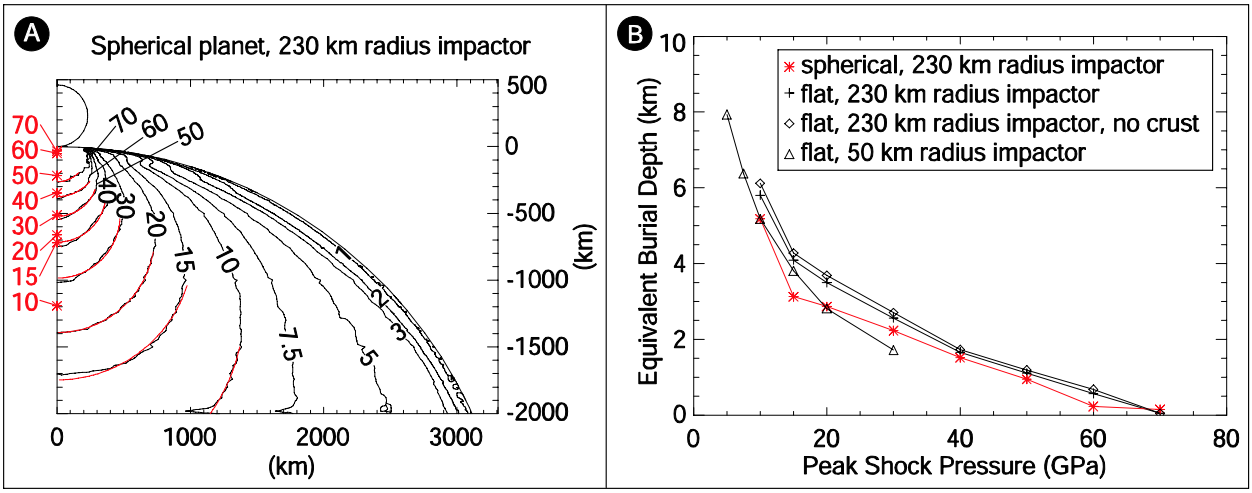

Figure S5. (A) Peak shock pressure contours (black lines) in GPa for the CTH simulation of a 230-km radius impactor onto a spherical Mars at 9 km/s. Semi-circles centered on the vertical centerline below the impact point (red lines) were fit to the pressure contours below the interference zone. The depths of the semi-circle centers are the equivalent depth of burial points for each pressure contour and are indicated by the red star symbols. No vertical exaggeration. (B) The equivalent burial depths for different pressures for four different CTH simulations are shown. With decreasing peak shock pressure the equivalent burial depth increases (see discussion of center of flow field in [*Croft*, 1980]); only for relatively high peak shock pressures (~60 GPa) is the equivalent burial depth approximately $0.7 \cdot r_{pr}$ [*Pierazzo, et al.*, 1997].

Table S4. Average shock pressure between 10 and 50 km depth on Mars from 3D-CTH calculations for a Hellas-type event.

Distance from the impact point along the surface (km)	r_{pr} *= 230 (km)*	r_{pr} *= 125 (km)*
250	54 (±17)	20 (±4.2)
500	17 (±1.5)	8.1 (±1.1)
750	8.6 (±1.1)	2.0 (±0.3)
1000	3.4 (±0.7)	1.1 (±0.2)
1250	2.1 (±0.4)	0.7 (±0.1)
1500	1.5 (±0.3)	0.6 (±0.1)

With standard deviations in parentheses. $\tau = r_{pr}/v_i$, v_i = 9 km/s, $d = 0.7 \cdot r_{pr}$.

References

Barnes, J., and P. Hut (1986), A hierarchical O(N log N) force-calculation algorithm, *Nature*, *324*, 446-449, doi:10.1038/324446a0.

Benz, W., A. G. W. Cameron, and H. J. Melosh (1989), The origin of the Moon and the single impact hypothesis III, *Icarus*, *81*, 113-131, doi:10.1016/0019-1035(89)90129-2.

Crawford, D. A. (1999), Adaptive mesh refinement in CTH Report SAND99-1118C, 10 pp, Sandia National Laboratory, Albuquerque NM.

Croft, S. K. (1980), Cratering flow fields: Implications for the excavation and transient expansion stages of crater formation, *Proc. Lunar Plan. Sci. Conf. 11th*, 2347-2378.

Dziewonski, A. M., and D. L. Anderson (1981), Preliminary reference Earth model, *PEPI*, *25* (4), 297-356, doi:10.1016/0031-9201(81)90046-7.

Holian, K. S. (1984), T-4 Handbook of Material Properties Data Bases, Vol. 1c: Equations of State Report LA-10160-MS, 382 pp, Los Alamos National Laboratory, Los Alamos, NM.

Kerley, G. I. (1993), Multiphase Equation of State for Iron, Sandia National Laboratories, Albuquerque, NM.

McGlaun, J. M., S. L. Thompson, and M. G. Elrick (1990), CTH: A 3-dimensional shock-wave physics code, *Int. J. Impact Eng.*, *10*, 351-360, doi:10.1016/0734-743X(90)90071-3.

Melosh, H. J. (2007), A Hydrocode Equation of State for SiO_2, *MAPS*, *42* (12), 2079-2098.

Pierazzo, E., A. M. Vickery, and H. J. Melosh (1997), A Reevaluation of Impact Melt Production, *Icarus*, *127*, 408-423, doi:10.1006/icar.1997.5713.

Valencia, D., R. J. O'Connell, and D. Sasselov (2006), Internal structure of massive terrestrial planets, *Icarus*, *181* (2), 545-554, doi:10.1016/j.icarus.2005.11.021.

Zuber, M. T. (2001), The crust and mantle of Mars, *Nature*, *412*, 220-227, doi:10.1038/35084163.